High-resolution TEM investigation of structure and composition of polar Pd/ZnO interfaces

Mitsuhiro Saito,[1,2,*] Thomas Wagner,[2] Gunther Richter,[2] and Manfred Rühle[2,†]
[1]*WPI Advanced Institute for Materials Research, Tohoku University, 2-1-1, Katahira, Aoba-ku, Sendai 980-8577, Japan*
[2]*Max-Planck-Institut für Metallforschung, Heisenbergstr. 3, D-70569 Stuttgart, Germany*
(Received 14 April 2009; revised manuscript received 23 August 2009; published 14 October 2009)

In several metal/oxide interfaces, it is well known that polar facet of the oxide influences the formation of a stable metal/oxide interface. However, the formation mechanism of such polar interface is still unclear. In this work, Pd/(0001)ZnO and Pd/$(000\bar{1})$ZnO interfaces were used as model systems to investigate the polar metal/oxide interfaces. High-resolution transmission electron microscopic (HRTEM) observation was performed on atomic scale. Quantitative analysis of the HRTEM image revealed specific local atomic structures near the polar interfaces. The Pd/(0001)ZnO interface is found to be terminated with Zn and only these Zn atoms were relaxed to compensate for the interfacial lattice mismatch as large as 18%. Moreover, the Zn atoms occupy lattice sites of the Pd crystal. On the other hand, the Pd/$(000\bar{1})$ZnO interface is terminated with O. In this case, the Pd crystal was relaxed to terminate dangling bonds of all terminating oxygen atoms. These results were complemented by semiquantitative *first principles* calculations, where the charge transfer across each interface could be analyzed. The different terminations and charge transfers across the interfaces preserved the total charge balance of the ZnO crystal. The relaxations of lattice mismatch at the interfaces formed chemically interactive geometries depending on the polarity of ZnO.

DOI: 10.1103/PhysRevB.80.134110 PACS number(s): 68.37.Og, 73.40.Ns, 31.15.A−

I. INTRODUCTION

Metal/oxide (M/O) systems are employed in various industrial applications, e.g., oxide-strengthened alloys, catalysts, Schottky barrier diodes, and metal-oxide-semiconductor field-effect transistors.[1,2] The interface between the metal and oxide play a key role in macroscopic properties.[2–5] In many cases, it is well known that stable M/O interfaces tend to grow on the polar facet of the oxide.[6–11] A detailed analysis of the local atomic structure of such a polar M/O interface is essential for understanding and improving their performance and functionality.[12–19]

ZnO is an II-VI wide-band-gap semiconductor and a promising candidate for electronic and optical devices.[20–22] ZnO crystallizes in the wurtzite structure with lattice parameters of $a=0.325$ nm and $c=0.521$ nm, resulting in a noncenter symmetric structure. The (0001)ZnO and $(000\bar{1})$ZnO surfaces are polar planes which can be terminated with either O or Zn. It is known that atomically flat polar {0001}ZnO surfaces result in electrical instability.[23] Actually, ZnO crystals grown in air do not possess a basal plane as a surface of the ZnO. When the {0001} surface is atomically flat and unreconstructed without charge transfer, the sum of the dipole moments caused by Zn-O atomic pairs cannot be annihilated along the c axis of ZnO; then, the electric field and the surface energy diverge to infinity.[24] Noguera suggested a stabilizing mechanism for the {0001}ZnO surface.[23] The intrinsic electrostatic field E has to be annihilated by means of an extrinsic electrostatic field $-E$ induced by a surface charge, $dq=\mp q/4$, where $q(=2e)$ is the typical ionic charge of Zn and O. The surface charge can be generated by (i) real surface charging, (ii) surface impurities, or (iii) virtual surface charging due to vacancies (partial coverage) of the topmost ions. According to studies for {0001}ZnO surfaces,[11,25–27] it was reported that the surface charge can be generated by the vacancies of the topmost ions. Jedrecy *et al.* quantified stoichiometry of a (0001)ZnO surface through the crystal truncation rod (CTR) measurements using x-ray diffraction. The CTR measurements revealed that the topmost atomic species is Zn and the Zn toplayer of the surface has the partial coverage of 75%.[25] Dulub *et al.* observed a (0001)ZnO surface by scanning-tunneling microscope (STM). The STM images show many triangular hollows and islands on the (0001)ZnO surface which has several specific sizes and a step height of $c/2$. All islands locally have stoichiometric ratio of 75:100=Zn:O.[26] Although Jedrecy *et al.* and Dulub *et al.* treated to the ZnO surface via different ways, the results concerning stoichiometry of the surfaces were identical. STM images taken by Parker *et al.* also showed many triangular hollows and islands with a step height of $c/2$ on the $(000\bar{1})$ZnO surface as well as on the (0001)ZnO surface.[27] The both surfaces seem to be stabilized by virtual charging due to vacancies of ions in the top layer.

There are several reports for the growth behavior of metal on such {0001}ZnO surfaces.[28–32] The stabilizing mechanism seems to be changed depending on the local atomic structure at the M/ZnO interface. Jedrecy *et al.* reported the growth behavior of silver thin film on the two polar faces of ZnO by surface x-ray diffraction (SXRD) technique.[28,29] On both surfaces, the Ag forms nanoclusters with (111) top facets in hexagon-on-hexagon epitaxy with $[10\bar{1}]_{Ag}\|[100]_{ZnO}$. Despite the high-lattice mismatch (11%), the Ag islands adopt their bulk parameter even in an initial stage of growth. It was concluded that the epitaxial-orientation relationship is favored by a quasiperfect coincidence of nine Ag cells on eight ZnO cell. Concerning the growth mode, flat-top Ag clusters were formed on both Zn- and O-terminated ZnO polar surfaces, which allow modeling of the system in the high coverage by a continuous Ag film with holes instead of isolated clusters. Ag spreads more significantly on the O-terminated face than on the Zn termination. Lin and Bristowe found O-terminated interface is stronger.[33] In addition, the large

period (9×8) Ag/ZnO coincidence superstructure with mismatch of 0.1% is energetically preferred. The local atomic geometry strongly influenced the work of separation with on-top site being preferred for the Ag-O bonding and the hcp-hollow site being preferred for the Ag-Zn bonding.

In the case of Cu/ZnO system, Jedrecy *et al.* revealed that copper aggregates into flat islands, with two orientation relationships, at 180° from each other: $(111)\mathrm{Cu}\|(000\bar{1})\mathrm{ZnO}$ with $[10\bar{1}]_{\mathrm{Ag}}\|[100]_{\mathrm{ZnO}}$ by SXRD data.[30] The islands are not strained on the substrate in spite of large lattice mismatch, even at very early growth stage. In addition, the ordered fraction of atoms in the top O plane is reduced by one quarter. It was considered that the Cu adatoms involved in Cu-O interaction could be responsible for the surface derelaxation through a charge transfer. Meyer and Marx found that partial Cu coverage forms strong adhesion of Cu atoms using a density-functional-theory calculation.[34] The binding energy sensitively depends on how charge neutrality of the polar surface is achieved.

Although the stabilization of ZnO with metal might be related to charge neutrality of ZnO and dependent on the kind of deposited metal, its mechanism remains unclear. This study has been devoted to the direct observation of polar Pd/ZnO interfaces because Pd is a nonreactive metal and the behaviors might be different from that of Ag and Cu. ZnO precipitates grown by internal oxidation of the Pd-Zn alloy possess extremely wide Pd/(0001)ZnO and Pd/$(000\bar{1})$ZnO interfaces compared to the other interfaces which are not parallel to the basal planes of ZnO.[9] This indicates that the existence of Pd influences the formation of a stable polar facet of the ZnO. The following scientific questions will be addressed for the Pd/ZnO interface: (i) orientation relationships between Pd and ZnO crystals, (ii) interfacial local atomic structure, (iii) terminating atomic species of ZnO, (iv) spatial occupancy of terminating atomic species at the interface, (v) nature of the interfacial bonding, (vi) structural differences for the different polar planes, (vii) growth behaviors, and (viii) mechanisms to form the Pd/ZnO polar interfaces. Pd/(0001)ZnO and Pd/$(000\bar{1})$ZnO interfaces were analyzed and compared on atomic scale by using a high-voltage high-resolution transmission electron microscope.

II. EXPERIMENTAL AND COMPUTATIONAL DETAILS

Single-crystalline substrates of ZnO were purchased from University Wafer Co. (MA, USA). All ZnO substrates were annealed in 1 atm pure oxygen environment for 3 h at 950 °C. Subsequently, the substrates were annealed in ultrahigh vacuum (UHV) environment at $\sim1\times10^{-7}$ Pa at 600 °C for 1 h to remove surface impurities. Pd films with thickness of 30 nm were separately grown by molecular-beam epitaxy (MBE) on both (0001)ZnO or $(000\bar{1})$ZnO surfaces at 600 °C in UHV environment of $\sim1\times10^{-7}$ Pa. First, in order to examine the influence of the polarity (termination), growth behaviors of Pd on (0001)ZnO and $(000\bar{1})$ZnO surfaces were observed by using atomic-force microscopy (AFM). Afterwards, for cross-sectional transmission electron microscopic (TEM) observation of the Pd/ZnO interface, TEM specimens were prepared by conventional thinning procedure[35] through grinding and ion milling with 3.8 keV.

The technical problems relating to HRTEM observation is image analysis for ZnO with extremely small lattice spacing of 0.114 nm [Fig. 1(a)]. Therefore, HRTEM micrographs of the Pd/ZnO interfaces were taken near the Scherzer defocus condition (df:−50 nm) using an ultrahigh voltage microscope JEOL JEM-ARM1250 (1.25 MeV).[36] Under this imaging condition, maximal point-to-point resolution of 0.12 nm can be attained. In order to extract three-dimensional atomic structure from the HRTEM images, the interfaces were observed along different zone axes tilted by 90° with respect to each other.

Second problem is the difficulty to interpret the image contrast near the interface where the periodicities of crystals are broken, A HRTEM images the projected specimen structure as a complicated interference pattern because the image is generated by a strong nonlinear process. Therefore, quantitative interpretation necessitates a comparison of experimental images with simulated images. The simulation can be carried out based on the multislice method.[37] Iterative digital-image-matching (IDIM) program package allows for the quantitative determination of not only the most likely imaging parameter but also the atomistic coordinates and spatial occupancies of atomic columns.[38] This is done by a numerical optimization routine. The experimental image is automatically compared with simulated images obtained by various parameters. The cross-correlation factor (XCF) can be used to quantify the agreement between the two images. When a normalized intensity at pixel (j,k) is defined as E_{jk}, S_{jk} in the experimental (E) [Fig. 1(b)] and simulated (S) [Fig. 1(c)] images, respectively, the XCF is given by the following Eq. (1). The residual error corresponding to disagreement [Fig. 1(d)] needs to be minimized.

$$\mathrm{XCF}(E,S)=\frac{\Sigma(E_{jk}-\bar{E})\cdot(S_{jk}-\bar{S})}{\sqrt{\left(\Sigma E_{jk}-\bar{E}\right)^2\cdot\left(\Sigma S_{jk}-\bar{S}\right)^2}},$$

$$\text{with}\ \sum=\sum_{j,k=1}^{nx.ny}. \tag{1}$$

This iteration of the set of parameters is repeated until the best agreement (maximum XCF) is reached. Typical values are larger than 90%. This represents the best achievable agreement between experimental and simulated conditions. Then, the most likely specimen structure can be known.

The interfacial local electronic nature was complemented by semiquantitative *first-principles* DVXα (Ref. 39) cluster calculation. Due to limitations in computer performance, cluster calculation is an appropriate method to simulate the electronic states of the system having incomplete three-dimensional periodicity in atomic arrangements such the Pd/ZnO interface without reasonably good matching. The cluster for the calculation was reduced to a representative structure with an executable size. Mulliken population analysis was performed to evaluate ionic charges, bond overlap

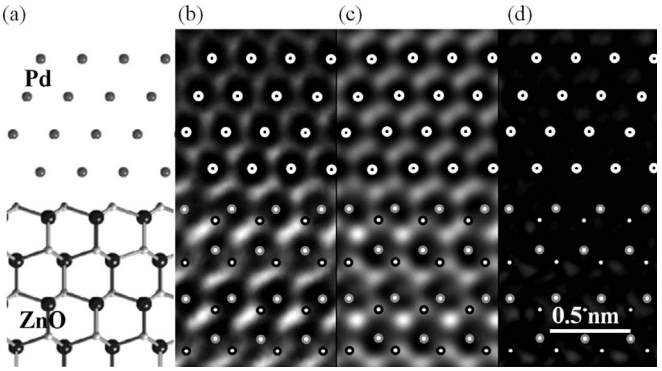

FIG. 1. (a) Projected structures of bulk Pd and ZnO crystals along $[\bar{1}10]_{Pd}\|[100]_{ZnO}$ zone axes, (b) one example of experimental HRTEM image of the Pd/(0001)ZnO interface, (c) simulated image optimized only for imaging parameters, and (d) difference image between the experimental and simulated images. In the difference image, the residual white contrast suggests mismatch between the experimental and simulated images.

populations, and net covalent charges in order to estimate interfacial bonding.

III. RESULTS AND DISCUSSION

A. Growth behavior of Pd on {0001}ZnO surfaces

The AFM images in Fig. 2 show that the Pd grain size of 300–1500 nm on the $(000\bar{1})$ZnO surface is larger than that of 100–400 nm on the (0001)ZnO surface and that the film thickness of 50–70 nm on the $(000\bar{1})$ZnO surface is not much different from that of 40–80 nm on the (0001)ZnO surface (nominal thickness of 30 nm estimated by the quartz thickness monitor of MBE). The channels between the Pd islands on both ZnO surfaces suggest an island-growth mode (nonwetting system) as expected due to the low reactivity of Pd. In the case of the $(000\bar{1})$ZnO surface, larger islands are formed and liquid-like coalescence is observed earlier since the growth rate and time are the same for both surfaces. This suggests that Pd atoms form a strong interfacial bonding on the $(000\bar{1})$ZnO surface. Furthermore, the cross-sectional

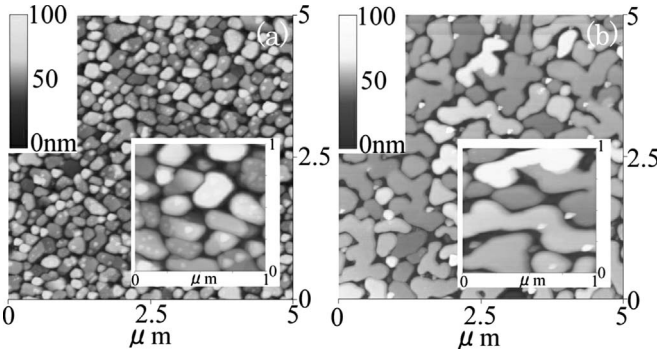

FIG. 2. AFM images of Pd islands grown on the (a) (0001)ZnO surface and (b) $(000\bar{1})$ZnO surface. The large image size is 5×5 μm and the inset image size is 1×1 μm.

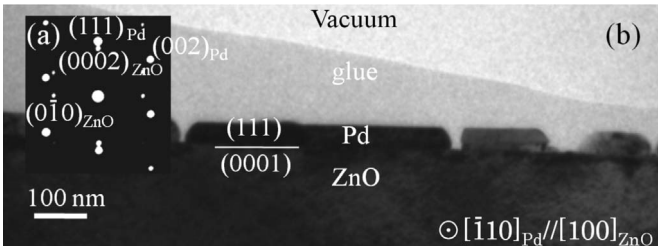

FIG. 3. (a) Selected-area-diffraction pattern and (b) conventional bright field image of the Pd/(0001)ZnO interface.

bright field TEM image of the Pd/(0001)ZnO interface in Fig. 3 shows that flat-top islands with thickness of 50–60 nm and the channels were formed. In Ag/(0001)ZnO system, flat-top islands with holes were found on both Zn(0001) and $O(000\bar{1})$ surfaces and a significant metallic spreading was observed on the O surface,[29] indicating the same behavior as in this work.

B. Lattice mismatch of Pd/{0001}ZnO interfaces

1. Orientation relationship

The diffraction pattern in Fig. 3(a) indicates the following well-defined epitaxial orientation relationships between Pd islands and the ZnO crystal for both Pd/(0001)ZnO interface and Pd/$(000\bar{1})$ZnO interface

$$(111)_{Pd}\|\{0001\}_{ZnO} \quad \text{and} \quad [\bar{1}10]_{Pd}\|[100]_{ZnO}.$$

Although the lattice mismatch is high (18%), there are site lattice coincidence that allow the Pd/ZnO epitaxy: seven unit cells of Pd match with six unit cells of ZnO at 1.2%. This gives rise to a super coincidence every 1.6 nm. It was reported in the Ag/ZnO system with large lattice mismatch of 12% that nine unit cells of Ag match with eight unit cells of ZnO in a way similar to the super coincidence every 2.6 nm.[28,29]

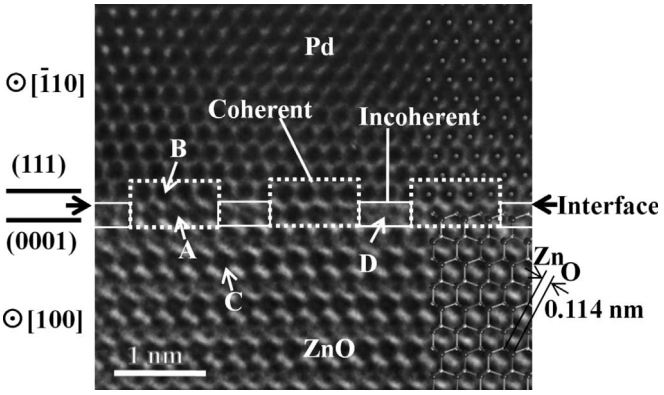

FIG. 4. Experimental HRTEM image of the Pd/(0001)ZnO interface. Coherent interface areas of the interfacial layer of ZnO show clearly resolved columns within the dotted white frame. The interface also possesses Incoherent interface areas which show diffusely imaged columns within the solid white frame. These incoherent interface areas are present periodically next to coherent interface areas.

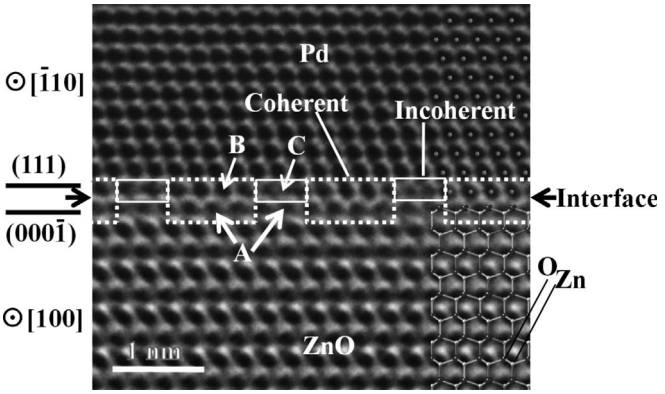

FIG. 5. Experimental image of the Pd/(000$\bar{1}$)ZnO interface. The terminating Pd layer also has an incoherent interface area with diffusely imaged columns within the solid white frame.

2. Super coincidence

Figure 4 shows a micrograph of the Pd/(0001)ZnO interface taken along the $[\bar{1}10]_{Pd}\|[100]_{ZnO}$ zone axes. Zn and Pd are imaged as having black contrast and O has gray contrast according to the simulation as shown in Fig. 1(c). The minimum-projected distance between Zn and O is 0.114 nm, close to the resolution. Therefore, the contrasts of Zn and O atoms are overlapped and look like one atomic column denoted by an A in Fig. 4 rather separated columns. Figure 4 shows that the image contrast of the atomic columns of the heavy Pd (denoted by B) is different from that of the A for the Zn-O atomic pair. The image clearly shows the difference in the diameter of the atomic columns between the Pd and ZnO regions, indicating that the Pd/ZnO interface is atomically abrupt and both crystals are directly bonded.

All Pd atoms on the interfacial layer denoted by the B in Fig. 4 are located at the lattice points of the perfect crystal of Pd. The ZnO region near the interface possesses "coherent interface areas" with clearly resolved ZnO columns denoted by A (within the dotted white frame). ZnO of this area has almost the same contrast and intensity as that in the bulk ZnO region denoted by C. However, the ZnO also has "incoherent interface areas" with diffusely imaged columns denoted by D (within the solid white frame only at the interfacial layer in Fig. 4). These incoherent interface areas exist alternatively next to the coherent interface areas. It can be seen that the total length of both the incoherent interface area (~0.5 nm) and the coherent interface area (~1.1 nm) is ~1.6 nm along the interface. This length matches the periodicity of the super coincidence of 1.6 nm.

Figure 5 shows a HRTEM image taken along the $[\bar{1}10]_{Pd}\|[100]$ zone axes of the Pd/(000$\bar{1}$)ZnO interface. The interface between Pd and ZnO is atomically flat. The main difference from the Pd/(0001)ZnO interface is that all the atoms next to the interface in the ZnO are located at the positions of the perfect crystal of ZnO denoted by A while the interfacial Pd layer shares both the coherent interface area with clearly resolved Pd column denoted by B and the incoherent interface area with diffusely imaged Pd contrast denoted by C. The total length of the incoherent interface area (~0.5 nm) and the coherent interface area (~1.1 nm) is about 1.6 nm along the interface. This length is same as that in the Pd/(0001)ZnO interface.

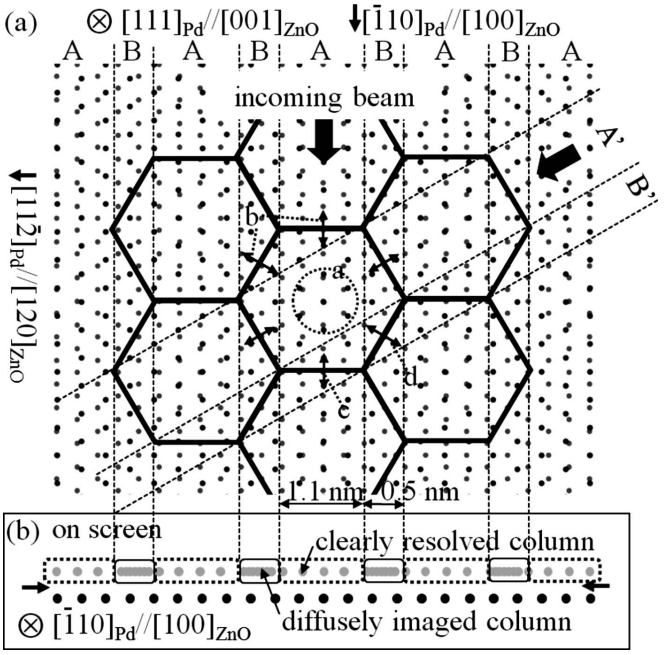

FIG. 6. (a) Schematic of interfacial atoms. In this dichromatic pattern, the black dots are ZnO and the gray dots Pd. A misfit dislocation can be expected on the hexagonal network and relaxation motion has to be perpendicular to the network. The region wherein the relaxation motion is parallel to the incoming beam direction is denoted by A and the region wherein the motion includes a component normal to the incoming beam is denoted by B. (b) The projected structure of the terminating atoms at the interface.

The repetition of the incoherent interface area and the coherent interface area observed in both interfaces can be explained by two-dimensional super coincidence between Pd and ZnO. Figure 6(a) shows a schematic of the terminating atoms of both Pd and ZnO, in the $\langle 0001\rangle_{ZnO}$ projection, assuming the same spacings in both bulk crystals. The spatial repetition of the Moiré pattern should be noted. The region enclosed by the circle "a" in Fig. 6(a) shows a better coincidence between the interfacial atoms of Pd and ZnO. Such regions exist periodically.

If the mismatched region is minimized, the atoms in the region with poor coincidence at the interface need to be moved. Then, misfit dislocations must be formed. A hexagonal dislocation network can be drawn by connecting the worst coincident positions, as shown in Fig. 6(a). The hexagonal network corresponds to the construction of a near-coincidence-site lattice.[40] Since shifts in the atoms are expected along the normal to the dislocation network denoted by "b" in Fig. 6(a), the relaxing directions "c" of the atoms in region A should include only the parallel component to the incoming *e*-beam direction along the $[\bar{1}10]_{Pd}\|[100]_{ZnO}$ zone axes. Since a HRTEM image yields a projected structure, for instance, the image of the terminating atoms at the Pd/(000$\bar{1}$)ZnO interface can be expected as shown in Fig. 6(b). The gray and black dots mean terminating Pd and O

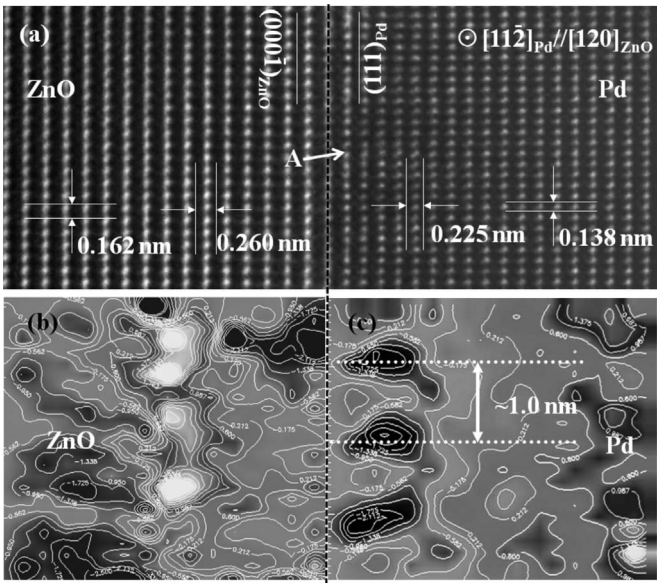

FIG. 7. (a) HRTEM image of the region close to the $Pd/(000\bar{1})ZnO$ interface taken along the $[112]_{Pd}\|[1\bar{1}00]_{ZnO}$ zone axes. [(b) and (c)] Contour map of strain field detected from the image of the ZnO and Pd region near the $Pd/(000\bar{1})ZnO$ interface by LADIA program package, respectively. Low (black) intensity indicates compressive stress while high (white) intensity indicates tensile stress.

atoms, respectively. The relaxation of atoms denoted by c in region A does not disturb the image of atomic columns on the screen as shown in Fig. 6(b), suggesting the formation of clearly resolved columns. On the other hand, the moving direction "d" in region B [Fig. 6(a)] possesses a component along the normal to the *e*-beam direction, indicating that the relaxation might form the diffusely imaged columns on the screen.

If this model for the generation of misfit dislocations is correct, the repeat unit of both regions A (~1.1 nm) and B (~0.5 nm) should be ~1.6 nm on the screen. Indeed, this agrees with the experimental value of 1.6 nm. Therefore, we can conclude that this relaxation model of the hexagonal network is valid. In spite of the large lattice mismatch of 18%, localization of the misfit was detected at both interfaces. This suggests that the degree of geometrical mismatch does not necessarily influence the existence of a misfit dislocation. We have to consider not the geometry but the bonding nature across the interface.

3. Relaxed crystal

Moreover, the relaxation behavior depends on the polarity of the oxide. In the $Pd/(000\bar{1})ZnO$ interface, the Pd crystal is relaxed to fit the lattice of ZnO. This is the typical behavior because oxide is more rigid. It was reported that the bulk lattice parameter is preserved in the $Cu/(000\bar{1})ZnO$ case and Ag/{0001}ZnO case.[28–30] In the case of the Pd/(0001)ZnO interface, however, the relaxation does not occur in Pd but rather in ZnO. Lattice relaxation of an oxide such as ZnO is rather unusual compared to the relaxation of Pd. In fact, relaxation in the bulk region of ZnO could not be seen even in the Pd/(0001)ZnO interface. It was observed only in the first Zn layer at the Pd/(0001)ZnO interface. The chemical environment around an atom at an interface is different from that of an atom in the bulk. At the interface, this different environment may affect the ionic and covalent bonding nature of the bonds between the terminating Zn and the neighboring O atoms. Then, the relaxation of only the first layer in an oxide such as ZnO can be explained at the Pd/(0001)ZnO interface.

The interfaces were investigated also for another zone axes, parallel to the $[11\bar{2}]_{Pd}\|[210]_{ZnO}$ zone axes and perpendicular to the first zone axes. Figure 7(a) shows a HRTEM image of the region close to the $Pd/(000\bar{1})ZnO$ interface. The interface could be recognized from the different lattice spacings between Pd and ZnO. An atomically flat interface with no strain field in the ZnO bulk region can be seen. The Pd region near the interface has white dots aligned with irregular interval denoted by A in Fig. 7(a). Furthermore, lattice distortion analysis was carried out for the HRTEM image in Fig. 7(a) using the LADIA (LAtice DIstortion Analysis) program package.[41] We can visualize the detailed strain field by measuring displacement from bulk lattice points on a HRTEM image. Figures 7(b) and 7(c) show contour map of the strain detected from the image of the ZnO and Pd region near the $Pd/(000\bar{1})ZnO$ interface, respectively. Compressive stress is indicated by low (black) intensity and tensile stress by high (white) intensity. Periodic strain fields in the bulk Pd region can be seen. Compressive stress periodically exists on the incoherent interface area. In the periodic arrangement parallel to the interface, a periodicity of 1.0 nm corresponds to the periodicity of super coincidence. The Pd layer relaxes within the first to about the sixth Pd layer. For the ZnO region, clear periodical strain cannot be seen. This result supports the idea that the Pd crystal relaxes at the $Pd/(000\bar{1})ZnO$ interface. Such a periodical strain field could not be seen in the Pd region near the Pd/(0001)ZnO interface.

C. Local atomic structure of Pd/{0001}ZnO interfaces

By simple inspection of the HRTEM images in Figs. 4 and 5 alone, it is difficult to determine the exact local atomic structures. We determined the local atomic structure by employing a quantitative image-analysis technique.

The appearance of an incoherent interface area suggests that atoms are relaxed along the direction that is not parallel to the incoming beam direction. It may be difficult to carry out an appropriate image simulation for the incoherent interface area because it requires a huge supercell. Therefore, the local atomic structure, together with the coherent interface area (dotted white frame in Figs. 4 and 5), was analyzed.

In the near coherent interface, three possible adsorption sites on ZnO surface might be energetically preferred by Pd adatoms. Figure 8(a) shows atomic structure of ZnO surface and possible adsorption sites occupied by Pd adatoms; on-top site, fcc hollow site, and hcp hollow site. The local atomic structure projected along the $[\bar{1}10]_{Pd}\|[100]_{ZnO}$ zone axes depends on the adsorption site occupied by Pd as shown

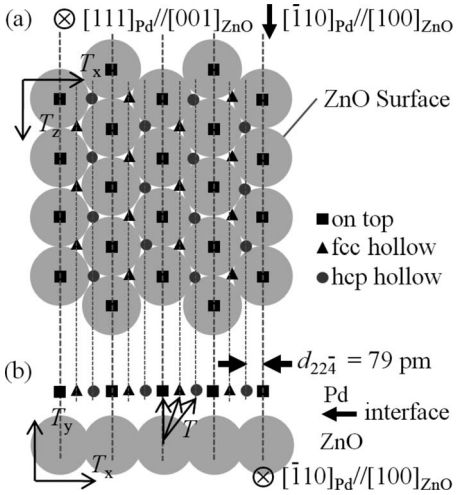

FIG. 8. (a) Energetically possible atomic geometries. Gray spheres are terminating atoms on ZnO surface. Solid squares, black spheres, and triangle mean possible adsorption sites occupied by Pd adatoms on the ZnO surface; the "on-top" sites, "fcc-hollow" sites, and "hcp-hollow" sites. (b) The possible projected structure when Pd adatoms are located at each site. We define the translation vector T as between the interfacial atom of ZnO and the nearest-neighboring interfacial Pd atom.

in Fig. 8(b). We define the translation vector T as between the interfacial atom of ZnO and the nearest-neighboring interfacial Pd atom to evaluate the most likely adsorption site. By measuring the translation vector and comparing the x component of the translation vector T with the lattice spacing $d_{22\bar{4}}$ of Pd (see Fig. 8), we can determine the local atomic structure.

First, a starting super cell, including the coherent interface area, was constituted by using an extension of the bulk lattice

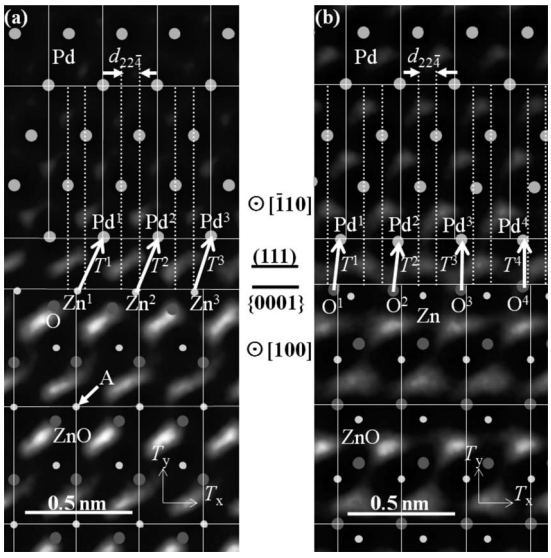

FIG. 9. The translation vectors T between each terminating atom of ZnO and the interfacial Pd atom are defined. The lattice points of bulk crystal are denoted by A. The best-fitting atomic structures in the image after optimization of the structure (a) near the Pd(0001)ZnO interface and (b) near the Pd/$(000\bar{1})$ZnO interface.

TABLE I. Translation vectors from the interfacial Zn atoms to the interfacial Pd atoms.

Translation vector	(T_x, T_y) [pm]	(T_x, T_y) [pm]
Optimization	Before	After
Zn^1-Pd^1	$(121, 229) \pm 25$	$(116, 241) \pm 25$
Zn^2-Pd^2	$(78, 229) \pm 25$	$(101, 243) \pm 25$
Zn^3-Pd^3	$(35, 229) \pm 25$	$(71, 252) \pm 25$

points denoted by the A in Fig. 9(a). The imaging parameters also should be optimized in bulk region of Pd and ZnO. We then can start to calculate the most possible local atomic structure (Fig. 8) via allowing only the relaxations of the atoms near the interface by the IDIM program package.[38]

1. Pd/(0001)ZnO interface

As a result, the Zn-terminated model yielded the best XCF value of 92.65%. In the local atomic structure after optimization [see Fig. 9(a)], the positions of the interfacial Pd atoms are the same as the lattice sites of the bulk region, indicating that the Pd atomic columns adjacent to the interface are not relaxed. However, the positions of the interfacial Zn atoms and the O atoms next to the Zn atoms are largely different from the lattice sites in the bulk ZnO. Table I indicates the x and y components of the translation vector T^i $(i=1-3)$ as between the interfacial Zn^i atom and the nearest-neighboring interfacial Pd^i atom before and after the optimization. Before the optimization, the translation vectors $|T_x|$ were distributed within 35–121 pm due to the large lattice mismatch of 18%. After the optimization, the average translation vectors $|T_x|$ were converged at 96 (± 25) pm which are closer to $d_{22\bar{4}}$ (79 pm) than $2d_{22\bar{4}}$ (158 pm) where the distance $d_{22\bar{4}}$ denotes the lattice spacing of Pd (see Fig. 8). This suggests that the interfacial Zn atoms fit in the Pd lattice sites (fcc hollow sites of the Pd crystal). This geometry can be understood by considering the general stacking geometry between fcc or hcp metals and also agree with the most stable atomic geometry in the Pd/(0001)ZnO interface calculated by Zaoui[42] and it is also similar to the results for Ag/(0001)ZnO calculated by Lin and Bristowe.[33]

Table I also shows that the average interfacial distances $|T_y|$ after the optimization is slightly increased to 245 (± 25) pm from the starting distance of 229 pm. The interfacial distance is slightly wider than the spacing d_{111} (225 pm) of Pd.

2. Pd/(000$\bar{1}$)ZnO interface

Figure 9(b) shows the most likely atomic structure on the image. In addition, the best XCF value (90.26%) can be obtained with the oxygen-terminated model. The O-Zn bonds of the interfacial O atoms are strongly bent and the interfacial Pd atoms are also shifted along the interface. The spacings between the interfacial O atoms are the same as that in bulk ZnO while the spacings between the interfacial Pd atoms are expanded in order to fit the lattice of ZnO. This

TABLE II. Translation vectors to the interfacial O atoms from the interfacial Pd atoms.

Translation vector	(T_x, T_y) [pm]	(T_x, T_y) [pm]
Optimization	Before	After
O^1-Pd^1	$(45,198)\pm 14$	$(12,204)\pm 14$
O^2-Pd^2	$(1,198)\pm 14$	$(25,223)\pm 14$
O^3-Pd^3	$(42,198)\pm 14$	$(3,220)\pm 14$
O^4-Pd^4	$(85,198)\pm 14$	$(3,207)\pm 14$

geometry can terminate the dangling bond of O atom along the c axis by the interfacial Pd atoms.

Table II shows the translation vectors T^i $(i=1-4)$ between the interfacial O^i atoms and the nearest-neighboring interfacial Pd^i atoms. Before the optimization, the translation vectors $|T_x|$ were distributed within 1–85 pm. After the optimization, the translation vectors $|T_x|$ converged at 11 (± 14) pm, which are closer to 0 pm than other possible lattice spacing of $d_{22\bar{4}}$ (79 pm) of Pd. This suggests that the Pd atoms are relaxed to fit on top of the lattice sites of ZnO.

Table II also shows that the average interfacial distance between two crystals after the optimization slightly increased to 214 (± 14) pm from the starting values of 198 pm. The interfacial distance after the optimization is narrower than the spacing d_{111} (225 pm) of Pd. This means that the ionic radius of the terminating O atom is less than that of the terminating Zn atom because the interfacial bonding distance (245 pm) between the Pd-Zn layers was larger than that between Pd-O layers. Inherently, in bulk ZnO, the ionic radius of O is much greater than that of Zn. This suggests an unusual ionic-charges transfer across the interface. Pd/(0001)ZnO interface. Lin *et al.* showed the influence on the translational state between the coherent interface without mismatch and the incoherent interface with small lattice mismatch by using theoretical calculation for the Ag/ZnO interface.[33] In the coherent interface, the translational state strongly influences the work of separation. In the incoherent interface, however, the translational state becomes less important and forms strongest bonding.

3. Atomic occupancies at the interface

The XCF value increased with adjusting partial occupancy of the atomic column of Zn along the zone axis at the Pd/(0001)ZnO interface. The best XCF of 92.65% was obtained for partial occupancy [Zn: 95% and Pd: 5%] at the terminating atomic column. Therefore, it can be concluded that the Pd/(0001)ZnO interface is terminated by Zn with the atomic occupancy of 95% (also including Pd with the atomic occupancy of 5% at the same atomic columns as Zn). It seems due to artifact. In the $Pd/(000\bar{1})$ZnO interface, the best XCF value (90.26%) can be obtained with full occupancy of the terminating oxygen along the zone axis [O: 100% and Pd: 0%].

The Pd deposition resulted in segregation of Zn atoms to the Pd/(0001)ZnO interface until ~95% coverage was reached. The coverage of the interfacial O layer in the $Pd/(000\bar{1})$ZnO interface is 100%. We determined occupancies of almost 100% by analyzing only the coherent interface area, except for the incoherent interface area at both interfaces. Unfortunately, in the incoherent interface areas, quantitative analysis was technically not possible. Nevertheless, the real spatial occupancy of the first layer of ZnO at the interface can be determined to be ~100% for all regions.

Preliminary experiments[11] on x-ray scattering and other studies[25–27] for the ZnO surface revealed that surface coverage of the topmost Zn atom was ~75%. Partial coverage provides a virtual surface charge to stabilize the ZnO crystal. If it can be assumed that an increase in the occupancy of the terminating Zn layer to 100% from the initial 75% is attributed to local segregation of Zn atoms to the coincident regions A [Fig. 6(a)], the poor coincident regions B around the coherent regions might have an occupancy below 75%, then the total real occupancy might still be 75% in all regions. However, this assumption is wrong. This is because {0001}ZnO and {111}Pd planes have three equivalent zone axes along the plane as shown in Fig. 6(a). Even if the interface was observed along the other equivalent zone axes, the same occupancy of 100% should be observed in the coherent interface area [region A′ in Fig. 6(a)]. The coherent interface area (region A′) observed along the other zone axis includes a part of the region B (resulting in the incoherent interface area) observed along the initial zone axis, as shown in Fig. 6(a). In spite of including region B in the observation along the initial zone axis, the occupancy should be 100%. This means that the interfacial Zn layer in all regions (even in region B) should have a real occupancy of 100%. Care must be taken that region B should not have a nominal occupancy of 100% due to the deviation from the atomic columns along the incoming beam direction. However, it should have a real occupancy of 100%. Although only the coherent interface area could be observed, fortunately, this was sufficient for determination of the real atomic occupancy. Therefore, the first Zn layer of ZnO at the Pd/(0001)ZnO interface possesses a real spatial occupancy of 100%. The same is true for the $Pd/(000\bar{1})$ZnO interface as well.

After Pd deposition, the spatial occupancy (coverage) of the interfacial Zn layer increased to nearly ~100% shown in this work. This means that in the case of the Pd/ZnO interface, there exists no virtual charge on the terminating {0001} planes of ZnO, indicating that it is unable to annihilate the intrinsic electric field of ZnO. This suggests that a real charge transfer must exist across the interfaces for stabilization of ZnO.

D. First-principles cluster calculation

The charge distribution and bonding nature at both Pd/ZnO interfaces were investigated by semiquantitative first-principles DVXα cluster calculations.[39] The calculations revealed the following.

The Pd-Zn bonding at the Pd/(0001)ZnO interface consists of a mixture of ionic $(Pd^{+0.05e-+0.29e}, Zn^{-0.86e--0.94e})$[bulk Zn:+1.1e] and covalent bonding (+0.14e−+0.17e) [bulk: ZnO:+0.24e] depending on possible local atomic geometries (on top, fcc hollow, and hcp

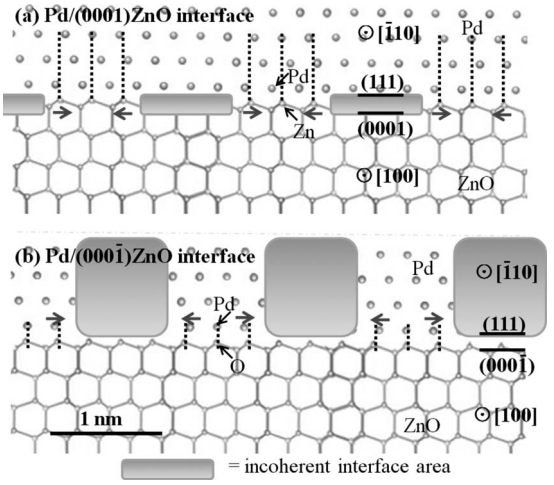

FIG. 10. (a) The most-stable local atomic structure of the Pd/(0001)ZnO interface wherein Zn sits at the fcc hollow site of the Pd lattice. At the interface, the ZnO crystal is relaxed to fit the Pd lattice due to the large lattice mismatch of 18% (the Pd atom in the third layer sits on top of the Zn atoms). (b) The most stable atomic structure of the Pd/(000$\bar{1}$)ZnO interface wherein Pd sits on top of the O of ZnO. At the interface, the Pd crystal is relaxed to fit the ZnO lattice.

hollow) between Pd and Zn. There was no strong difference in the local electronic states between all possible atomic geometries. This insensitivity to the atomic geometry can be attributed to the metal-like character of the interfacial bonding. Surprisingly, the interfacial Pd atoms are positively charged while the interfacial Zn atoms are negatively charged. On the other hand, the Pd-O bonding at the Pd/(000$\bar{1}$)ZnO interface consists of ionic bonding ($Pd^{-0.08e--0.56e}$,$O^{+1.59e-+1.63e}$) [bulk O:−1.1e] without a covalent character (+0.00e−+0.06e) [bulk ZnO:+0.24e]. The interfacial bonding of the Pd/(000$\bar{1}$)ZnO interface was sensitive to the location of Pd on ZnO. The location at which the Pd sits on top of O provides very strong ionic bonding ($Pd^{-0.56e}$,$O^{+1.61e}$), which is quite different from that at other locations. This sharp sensitivity to the local atomic geometry can be attributed to an asymmetric orbital around the O ion of ZnO. The dangling bond of O at the interface can be terminated by the arrangement of the interfacial Pd. The interfacial Pd is negatively charged while the interfacial O positively charged.

The differences between the Pd/(0001)ZnO interface and the Pd/(000$\bar{1}$)ZnO interface are the interfacial bonding type, charge of the interfacial atom, and the most stable local atomic geometry as shown in Fig. 10. Lin and Bristowe revealed Ag-Zn bond and Ag-O bond in Ag/{0001}ZnO interface.[33] The bonding types and stable geometries are similar to those determined in this work. It is quite unusual for ZnO that O is positively charged while Zn is negatively charged. This can be explained by considering the stabilizing mechanism of {0001}ZnO surfaces. The Pd/ZnO interfaces do not possess the virtual charges caused by vacancies on the {0001}ZnO topmost layer or any impurities to stabilize ZnO, indicating that it is unable to annihilate an intrinsic electric field E.[23] This suggests that real charge transfer must occur across the interfaces to maintain the total charge balance of ZnO. The real charging seems to annihilate the intrinsic electric field. Then, the ZnO crystal with atomically flat {0001} facets can stabilize by the real charging, even with Pd and without partial missing of the terminating layer of ZnO.

IV. CONCLUSIONS

Bonding between Pd and ZnO generally appears to be weak because Pd is a nonreactive metal, shows island growth mode, and it is hard to oxidize Pd. Such weak interfacial bonding does not affect the total energy of a Pd/ZnO system. On the other hand, ZnO with {0001} facets is very unstable and surface energy can diverge to infinity due to residual dipole moments. ZnO allows to decreasing largely the total energy of the system by compensating for the charge balance. Depending on the polarity, the terminating atomic species and the interfacial charges are adjusted in such a manner that the total energy of the Pd/ZnO system (especially, the surface energy of ZnO) is minimized. This global mechanism seems to be related to "the image charge theory"[19] wherein an image charge in a metal allows for the annihilation of an intrinsic electric field (in the metal) generated by the oxide. This also results in the establishment of an interfacial local structure that preserves high geometrical coherency (partially coherent interface) and chemically interactive geometry as a function of interfacial termination in this Pd/ZnO system.

ACKNOWLEDGMENTS

This work was mainly supported by the Max Planck Gesellschaft and Graduiertenkolleg Innere Grenzflächen (Deutsche Forschung Gemeinschaft). Partial support by Kakenhi (Grant No. 20860014) is acknoweledged. I also wish to thank F. Phillipp, H. Ichinose, and Y. Ikuhara for valuable discussions and also U. Salzberger, M. Kelsch, M. Pudleiner, and R. Höschen for specimen preparation and set up of the HRTEM.

*saito@wpi-aimr.tohoku.ac.jp
†ruehle@mf.mpg.de

[1] U. Grossner, S. Gabrielsen, T. M. Borseth, J. Grillenberger, A. Y. Kuznetsov, and B. G. Svensson, Appl. Phys. Lett. **85**, 2259 (2004).
[2] H. Endo, M. Sugibuchi, K. Takahashi, S. Goto, S. Sugimura, K. Hane, and Y. Kashiwaba, Appl. Phys. Lett. **90**, 121906 (2007).
[3] H. K. Kim, S. H. Han, T. Y. Seong, and W. K. Choi, Appl. Phys. Lett. **77**, 1647 (2000).
[4] M. W. Allen, M. M. Alkaisi, and S. M. Durbin, Appl. Phys. Lett.

89, 103520 (2006).
[5] M. W. Allen and S. M. Durbin, Appl. Phys. Lett. **92**, 122110 (2008).
[6] W. Mader, Z. Metallk. **80**, 139 (1989).
[7] H. Ichinose, H. Ishii, T. Ichimori, and Y. Ishida, in *Proceedings of the ICEM 13* (Les Editions de Physique des Ulis, France, 1994), Vol. 2A, p. 279.
[8] H. B. Groen and J. T. M. De Hosson, Scr. Mater. **38**, 769 (1998).
[9] K. Murakami, M. Saito, E. Takuma, and H. Ichinose, J. Electron Microsc. **52**, 27 (2003).
[10] T. Ichimori, Ph.D. thesis, The University of Tokyo, 1996.
[11] M. Saito, Ph.D. thesis, Universität Stuttgart, 2005.
[12] M. Rühle, A. G. Evans, M. F. Ashby, and J. P. Hirth, *4. Acta-Scripta Metallurgica Proc* (Pergamon, New York, 1990).
[13] M. Rühle, J. Eur. Ceram. Soc. **16**, 353 (1996).
[14] M. W. Finnis, J. Phys.: Condens. Matter **8**, 5811 (1996).
[15] F. S. Ohuchi and M. Kohyama, J. Am. Ceram. Soc. **74**, 1163 (1991).
[16] S. B. Sinnott and E. C. Dickey, Mater. Sci. Eng., R. **43**, 1 (2003).
[17] Y. Ishida, J. Wang, and T. Suga, Acta Metall. Mater. **40**, S289 (1992).
[18] Y. Ikuhara, P. Pirouz, A. H. Heuer, S. Vadavalli, and C. P. Flynn, Philos. Mag. A **70**, 75 (1994).
[19] F. Ernst, Mater. Sci. Eng., R. **14**, 97 (1995).
[20] D. M. Bagnall, Y. F. Chen, Z. Zhu, T. Yao, S. Koyama, M. Y. Shen, and T. Goto, Appl. Phys. Lett. **70**, 2230 (1997).
[21] A. Tsukazaki, A. Ohtomo, T. Onuma, M. Ohtani, T. Makino, M. Sumiya, K. Ohtani, S. F. Chichibu, S. Fuke, Y. Segawa, H. Ohno, H. Koinuma, and M. Kawasaki, Nature Mater. **4**, 42 (2005).
[22] S. J. Pearton, D. P. Norton, K. Ip, Y. W. Heo, and T. Steiner, J. Vac. Sci. Technol. B **22**, 932 (2004).
[23] C. Noguera, J. Phys.: Condens. Matter **12**, R367 (2000).
[24] P. W. Tasker, J. Phys. C **12**, 4977 (1979).
[25] N. Jedrecy, M. Sauvage-Simkin, and R. Pinchaux, Appl. Surf. Sci. **162-163**, 69 (2000).
[26] O. Dulub, U. Diebold, and G. Kresse, Phys. Rev. Lett. **90**, 016102 (2003).
[27] T. M. Parker, N. G. Condon, R. Lindsay, F. M. Leibsle, and G. Thornton, Surf. Sci. **415**, L1046 (1998).
[28] N. Jedrecy, G. Renaud, R. Lazzari, and J. Jupille, Phys. Rev. B **72**, 195404 (2005).
[29] N. Jedrecy, G. Renaud, R. Lazzari, and J. Jupille, Phys. Rev. B **72**, 045430 (2005).
[30] N. Jedrecy, S. Gallini, M. Sauvage-Simkin, and R. Pinchaux, Phys. Rev. B **64**, 085424 (2001).
[31] T. Nagata, J. Volk, Y. Yamashita, H. Yoshikawa, M. Haemori, R. Hayakawa, M. Yoshitake, S. Ueda, K. Kobayashi, and T. Chikyow, Appl. Phys. Lett. **94**, 221904 (2009).
[32] M. Ay, A. Nefedov, and H. Zabel, Surf. Sci. **600**, 5062 (2006).
[33] Z. Lin and P. Bristowe, Phys. Rev. B **75**, 205423 (2007).
[34] B. Meyer and D. Marx, Phys. Rev. B **69**, 235420 (2004).
[35] A. Strecker, U. Salzberger, and J. Mayer, Prakt. Metallogr. **30**, 482 (1993).
[36] F. Phillipp, R. Höschen, M. Osaki, G. Möbus, and M. Rühle, Ultramicroscopy **56**, 1 (1994).
[37] P. A. Stadelmann, Ultramicroscopy **21**, 131 (1987).
[38] G. Möbus, Ultramicroscopy **65**, 205 (1996).
[39] H. Adachi, M. Tsukada, and C. Satoko, J. Phys. Soc. Jpn. **45**, 875 (1978).
[40] D. M. Hwang, T. S. Ravi, R. Ramesh, S. W. Chan, C. Y. Chen, and L. Nazar, Appl. Phys. Lett. **57**, 1690 (1990).
[41] K. Du, Y. Rau, N. Y. Jin-Phillipp, and F. Phillip, J. Mater. Sci. Technol. **18**, 135 (2002).
[42] A. Zaoui, Phys. Rev. B **69**, 115403 (2004).